Journal of Hazardous Materials 203–204 (2012) 244–250

Contents lists available at SciVerse ScienceDirect

Journal of Hazardous Materials

journal homepage: www.elsevier.com/locate/jhazmat

Titanium dioxide–gold nanocomposite materials embedded in silicate sol–gel film catalyst for simultaneous photodegradation of hexavalent chromium and methylene blue

Alagarsamy Pandikumar, Ramasamy Ramaraj*

Centre for Photoelectrochemistry, School of Chemistry, Madurai Kamaraj University, Madurai 625021, India

ARTICLE INFO

Article history:
Received 22 June 2011
Received in revised form 2 December 2011
Accepted 5 December 2011
Available online 13 December 2011

Keywords:
Aminosilicate sol–gel
TiO_2–Au nanocomposite
Photocatalyst
Chromium(VI) reduction
Methylene blue oxidation
Advanced oxidation–reduction process

ABSTRACT

Aminosilicate sol–gel supported titanium dioxide–gold (EDAS/$(TiO_2–Au)_{nps}$) nanocomposite materials were synthesized by simple deposition–precipitation method and characterized. The photocatalytic oxidation and reduction activity of the EDAS/$(TiO_2–Au)_{nps}$ film was evaluated using hexavalent chromium (Cr(VI)) and methylene blue (MB) dye under irradiation. The photocatalytic reduction of Cr(VI) to Cr(III) was studied in the presence of hole scavengers such as oxalic acid (OA) and methylene blue (MB). The photocatalytic degradation of MB was investigated in the presence and absence of Cr(VI). Presence of Au_{nps} on the $(TiO_2)_{nps}$ surface and its dispersion in the silicate sol-gel film (EDAS/$(TiO_2–Au)_{nps}$) improved the photocatalytic reduction of Cr(VI) and oxidation of MB due to the effective interfacial electron transfer from the conduction band of the TiO_2 to Au_{nps} by minimizing the charge recombination process when compared to the TiO_2 and $(TiO_2–Au)_{nps}$ in the absence of EDAS. The EDAS/$(TiO_2–Au)_{nps}$ nanocomposite materials provided beneficial role in the environmental remediation and purification process through synergistic photocatalytic activity by an advanced oxidation–reduction processes.

1. Introduction

Titanium dioxide–gold nanocomposite materials have received greater attention because of their interesting optical, electronic, long time stability and excellent catalytic activity [1–6]. The titanium dioxide–gold nanomaterials ($(TiO_2–Au)_{nps}$), due to their wide and tunable band gap [7], find wide range of applications in the area of photocatalysis [8], electrocatalysis [9], sonocatalysis [10], electrochromic devices [11], photoelectrochemical cells [12,13], dye-sensitized solar cells [14], biosensors [15] and gas sensors [16–18]. Noble metal nanoparticles such as Au, Ag, Pt and Ir deposited on the surface of the $(TiO_2)_{nps}$ exhibit greater catalytic activity than that of the $(TiO_2)_{nps}$. The metal nanoparticles on $(TiO_2)_{nps}$ surface act as an electron sink for the photoinduced charge carriers and enhance the interfacial charge transfer process and minimize the charge recombination [19,20].

The hexavalent chromium (Cr(VI)) is a major pollutant added to the environment from the contaminated waters discharged from the electroplating industries, leather tanneries, paint and pigment industries. The Cr(VI) is highly toxic to most of the living organisms when the Cr(VI) concentration level is higher than 0.05 ppm. In contrast, the trivalent chromium (Cr(III)) is less toxic and one of the essential nutrient for body function. Hence the reduction of the Cr(IV) ions into Cr(III) ions received great attention in the environment purification processes [21–43]. Methylene blue (MB) is an organic dye pollutant discharged from dyeing industries. The dye contaminated water can affect the aquatic environments seriously. Removal of Cr(VI) and MB is a great challenge and several methods were reported for the removal of these pollutants [38]. Among them, the photocatalytic purification is economically viable, facile and effective one.

In the past decade the photocatalytic removal of Cr(VI) was studied by employing various photocatalysts, such as nano TiO_2 [21,22], in the presence of phenolic compounds [23,24], oxalic acid and EDTA [25], formic acid [26], ammonium and formate ions [27], salicylic acid [28], AO7 and rhodamine B [29], di-n-butyl phthalate [30], rotating TiO_2 mesh [31], sulphate modified TiO_2 in the presence of EDTA [32], TiO_2–BDD in the presence of RY15 [33], sol–gel derived TiO_2 thin film [34], ZnO in the presence of alizarin red-S [35] and methanol [36], polyoxomatalates in the presence of SA [37], rhodhamine B, metheylene blue and AO7 [38], neodymium-doped TiO_2 [39], Ag loaded TiO_2 [40], iron doped TiO_2 in the presence of NO_2^- [41], WO_3 doped TiO_2 nanotube in the presence of citric acid [42], organics acid modified TiO_2 [43], and Au_{nps} embedded TiO_2 framework in the presence of phenol [9].

In the present investigation, aminosilicate sol–gel supported $(TiO_2–Au)_{nps}$ were synthesized by deposition–precipitation method. The functionalized silicate sol–gel acts as a solid support

* Corresponding author.
E-mail address: ramarajr@yahoo.com (R. Ramaraj).

0304-3894/$ – see front matter © 2011 Elsevier B.V. All rights reserved.
doi:10.1016/j.jhazmat.2011.12.019

and provides stability to the embedded semiconductor–metal nanocomposite materials and facilitates the preparation of the solid phase photocatalyst in the film form. The photoinduced Cr(VI) ions reduction process plays a significant role in the synergistic and simultaneous acceleration of decomposition and mineralization of MB dye when EDAS/$(TiO_2–Au)_{nps}$ film was used. The present study shows one step forward process to improve the efficiency of the photocatalytic reduction and oxidation of Cr(VI) and MB, respectively by EDAS/$(TiO_2–Au)_{nps}$ embedded in aminosilicate sol–gel film. When the photoreduction of toxic Cr(VI) ions is carried out at the $(TiO_2–Au)_{nps}$ system, the reduction of Cr(VI) proceeds slowly. If the reduction is coupled with the photocatalytic oxidation of some organic compounds (organic dye), the reduction of Cr(VI) is promoted significantly in addition to the photodegradation of the organic compounds leading to the effective decrease in the charge recombination process at the $(TiO_2–Au)_{nps}$, called advanced oxidation–reduction processes.

2. Experimental

2.1. Chemicals

TiO_2 (Degussa P-25) (Evonik industries, Germany), hydrogen tetrachloroaurate trihydrate ($HAuCl_4.3H_2O$), N-[3-(trimethoxysilyl)propyl]ethylenediamine (EDAS) and methylene blue (MB) (Aldrich), potassium dichromate ($K_2Cr_2O_7$) and oxalic acid (OA) (Merck) were used as received and all the other chemicals used in this work were of analytical grade.

2.2. Synthesis of EDAS/$(TiO_2–Au)_{nps}$ nanocomposite materials

EDAS aminosilicate sol–gel functionalized TiO_2 was prepared by dispersing 1 g of TiO_2 (P-25) in a solution containing 30 mL of ethanol, 1.3 g of water, 0.7 g of aqueous ammonium solution (25 wt.%), and 0.6 g of EDAS were added. The reaction mixture was subjected to sonication for 1 h and then stirred at room temperature for 12 h. Then the mixture was purified by removing the excess EDAS and water or ammonia by repeated centrifugation and redispersion of the residue in absolute ethanol five times and dried under in vacuum at 80 °C for 10 h. The aminosilicate sol–gel (EDAS) supported $(TiO_2–Au)_{nps}$ nanocomposite materials was prepared by deposition–precipitation method. Briefly, 100 mL aqueous solution of 4.2×10^{-3} M $HAuCl_4$ was heated to 80 °C followed by the pH of the reaction mixture was adjusted to 7 by careful addition of 1 M NaOH. Then 1 g of EDAS functionalized TiO_2 was dispersed homogeneously into the solution and again pH was readjusted to 7 using 1 M NaOH. The reaction mixture was vigorously stirred for 2 h at 80 °C. The EDAS supported $(TiO_2–Au)_{nps}$ nanomaterials (EDAS/$(TiO_2–Au)_{nps}$) were gathered by repeated centrifugation (10,000 rpm for 15 min) and washed with 100 mL of double distilled water under stirring for 10 min at 50 °C. The synthesized EDAS/$(TiO_2–Au)_{nps}$ was dried under vacuum at 100 °C for 2 h in order to remove the moisture completely. During the preparation of EDAS/$(TiO_2–Au)_{nps}$), it was found that the addition of 4.2×10^{-3} M $HAuCl_4$ to the EDAS/TiO_2 lead the clear formation of the EDAS/$(TiO_2–Au)_{nps}$) (1.08 wt.% of Au on TiO_2) nanocomposite material and the surface plasmon band due the formation of Au nanoparticles on TiO_2 was observed (Fig. 1). The EDAS/$(TiO_2–Au)_{nps}$ nanocomposite material with 1.08 wt.% Au on TiO_2 was used for the photocatalysis studies. The change in $HAuCl_4$ concentration did not lead to the clear formation of EDAS/$(TiO_2–Au)_{nps}$ and sedimentation of brownish black color materials was observed. The surface plasmon band due the formation of Au nanoparticles on TiO_2 was not observed for these materials. For comparison, the same protocols was used to prepare bare $(TiO_2–Au)_{nps}$ in the absence of EDAS.

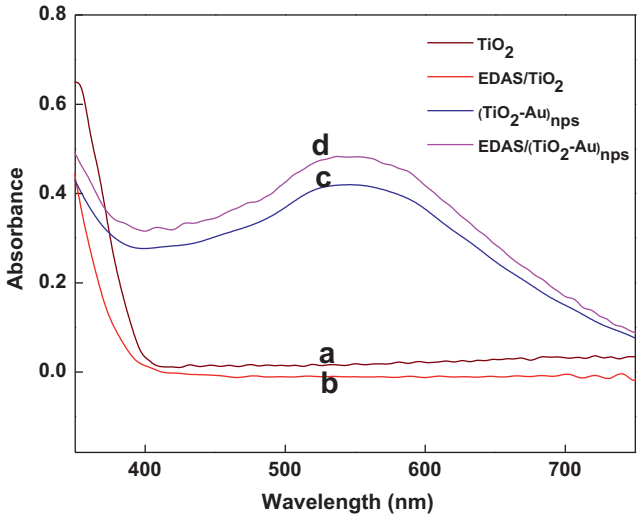

Fig. 1. Diffuse reflectance spectra of $(TiO_2)_{nps}$ (P-25) (a), EDAS/$(TiO_2)_{nps}$ (b), $(TiO_2–Au)_{nps}$ (c) and EDAS/$(TiO_2–Au)_{nps}$ (d) nanomaterials powders annealed at 450 °C.

2.3. Characterization of EDAS/$(TiO_2–Au)_{nps}$ nanocomposite material

The synthesized EDAS sol–gel supported $(TiO_2–Au)_{nps}$ nanocomposite materials were characterized by various techniques. Before characterization, the sample were annealed at 250 °C at a heating rate of 10 °C per minute and then maintained at 250 °C for 4 h. The diffuse reflectance spectra were recorded using $BaSO_4$ as a reference on Agilent 8453 diode array UV–visible spectrophotometer equipped with a Lab-Sphere diffuse reflectance accessories. Transmission electron microscopic (TEM) images were recorded using JEOL 3010 high resolution transmission electron microscope with operating voltage of 300 kV. Scanning electron microscopic (SEM) images were recorded using Carl Zeiss scanning electron microscope. Energy-dispersive X-ray spectroscopic (EDAX) analysis was carried out by FEI Quanta FEG 200 scanning electron microscope. X-ray diffraction (XRD) pattern was recorded on a Bruker AXS D8 Advance with Cu Kα radiation. Brunauer–Emmett–Teller (BET) surface area analysis were carried out using Micrometrics Gemini 2375 surface area analyzer *via* nitrogen (N_2) adsorption–desorption, using a single-point method after degassing the nanomaterials by flowing N_2 at 200 °C for 2 h.

2.4. Photocatalytic studies and analysis

The photocatalyst film was prepared by dispersing 750 mg of synthesized EDAS/$(TiO_2–Au)_{nps}$ nanomaterials in 5 mL ethanol and then sonicated for 5 min to ensure the homogeneous dispersion. The colloidal solution was coated as a film on a glass plate (1 cm^2) by casting a known volume of the solution and was allowed to dry in air at room temperature. Then the film was annealed at 450 °C for 30 min. For comparison, TiO_2 (P-25) film and $(TiO_2–Au)_{nps}$ in the absence of EDAS were also fabricated using the same procedure. The photocatalytic studies were carry out in a glass cell system at room temperature. The EDAS/$(TiO_2–Au)_{nps}$ or $(TiO_2)_{nps}$ or $(TiO_2–Au)_{nps}$ film coated glass plate was immersed into a photolysis cell containing a mixture of 0.4 mM $K_2Cr_2O_7$ and 4 mM MB and then irradiated with a light source. Before illumination, nitrogen was purged into the reaction mixture for 30 min in dark. The reaction mixture was stirred at a constant speed during

illumination. A 450 W Xenon lamp was used as the light source with a water filter cell (6 cm path length with pyrex glass windows) to cut off the far UV and IR radiations (Fig. S1). This water filter cell transmitted light from ~340 nm onwards. The sample aliquots were taken from the reaction sample at regular time intervals and were tested for dye degradation using spectrophotometer [44]. The Cr(VI) ions were estimated by diphenylcarbazide method at 540 nm by analyzing the complex formed upon the addition of colorimetric reagent 1,5-diphenylcarbazide [45,46].

3. Results and discussion

3.1. Spectral characterization of $(TiO_2–Au)_{nps}$ nanocomposite material

The present synthetic route for the preparation of EDAS/$(TiO_2–Au)_{nps}$ nanocomposite material is a simple procedure and, the affinity between the Au_{nps} and the amine groups in the EDAS plays a role in the formation of the $(TiO_2–Au)_{nps}$ nanocomposite material. The binding of silane on the surface of $(TiO_2)_{nps}$ has been well understood [13]. The lone pair of electrons present in the oxygen on the $(TiO_2)_{nps}$ surface's native hydroxyl acts as a nucleophile towards the electron deficient silicon in the EDAS and the silane is anchored on the TiO_2 surface [13]. The Au(III) ions bind to those aminosilane molecules undergo reduction to form Au_{nps}. The $(–NH_2\cdots Au_{nps})$ interaction is apparently sufficient to increase the local concentration of aminosilane around the Au_{nps} surface and to induce condensation and cross-linking of adjacent silanols and thus creating stable EDAS/$(TiO_2–Au)_{nps}$ nanocomposite material.

The diffuse reflectance spectra (DRS) of $(TiO_2)_{nps}$ (P-25) (a), EDAS modified $(TiO_2)_{nps}$ (b), $(TiO_2–Au)_{nps}$ (c) and EDAS silicate sol–gel supported $(TiO_2–Au)_{nps}$ (EDAS/$(TiO_2–Au)_{nps}$) (d) were recorded for powder samples annealed at 250 °C and 450 °C and are given in Fig. S2 and Fig. 1. The absorption spectral behavior of the samples annealed at 250 °C (Fig. S2) and 450 °C (Fig. 1) did not show any observable change in the absorption band. The DRS of the EDAS/$(TiO_2–Au)_{nps}$ films annealed at 250 °C and 450 °C were recorded and are given in Fig. S3. The DRS spectra (Fig. S3) did not show any change in the absorption band. The absorbance edge of the $(TiO_2–Au)_{nps}$ (Fig. 1) is significantly enhanced the light absorption in both UV and visible region. The absorption edge shifted towards longer wavelength when compared to the $(TiO_2)_{nps}$ (P-25) and EDAS modified $(TiO_2)_{nps}$ indicating a decrease in the band-gap of the EDAS/$(TiO_2–Au)_{nps}$. The band-gap energy values of bare TiO_2 and EDAS/$(TiO_2–Au)_{nps}$ are calculated by using *Taucs* plot method [7]. The band-gap energy values of $(TiO_2)_{nps}$ (P-25), EDAS/$(TiO_2)_{nps}$ and EDAS/$(TiO_2–Au)_{nps}$ were calculated as 3.2, 3.32 and 3.19 eV, respectively. The measured band-gap energy of EDAS/$(TiO_2)_{nps}$ (3.32 eV) showed a blue shift of 0.12 eV when compared to bare $(TiO_2)_{nps}$ (P-25) (3.2 eV). This is mainly attributed to the interaction between the support material (aminosilicate matrix) and the $(TiO_2)_{nps}$ [47]. For EDAS silicate sol–gel supported $(TiO_2–Au)_{nps}$, the band gap energy was found to be 3.19 eV with a small red shift of 0.01 and 0.13 eV when compared to the bare $(TiO_2)_{nps}$ and EDAS/$(TiO_2)_{nps}$. It clearly indicates the strong interaction and intragap formed between $(TiO_2)_{nps}$ and Au_{nps} [7]. The capping of Au_{nps} on the surface of $(TiO_2)_{nps}$ brings down the absorbance band edge of $(TiO_2)_{nps}$ near to the visible region [48]. It is expected that the Au_{nps}, a good conductor, could facilitate the rapid transfer of

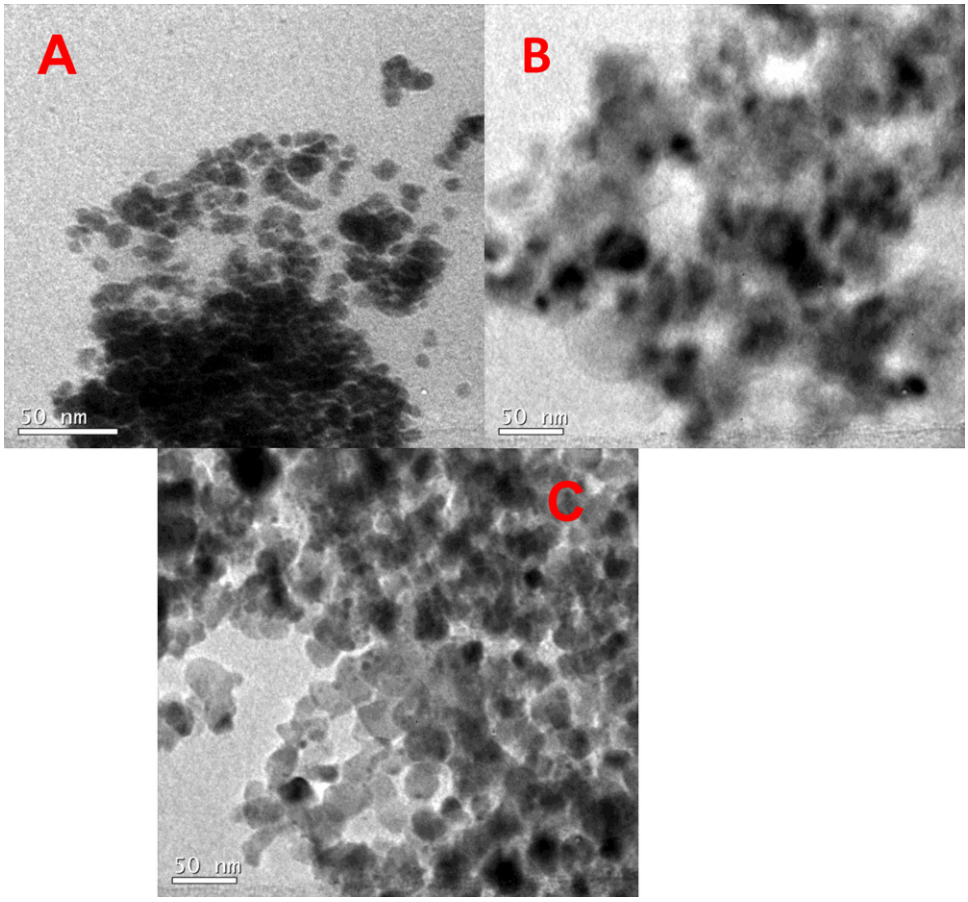

Fig. 2. TEM images of $(TiO_2)_{nps}$ (P-25) (A), $(TiO_2–Au)_{nps}$ (B) and EDAS/$(TiO_2–Au)_{nps}$ (C) nanomaterials.

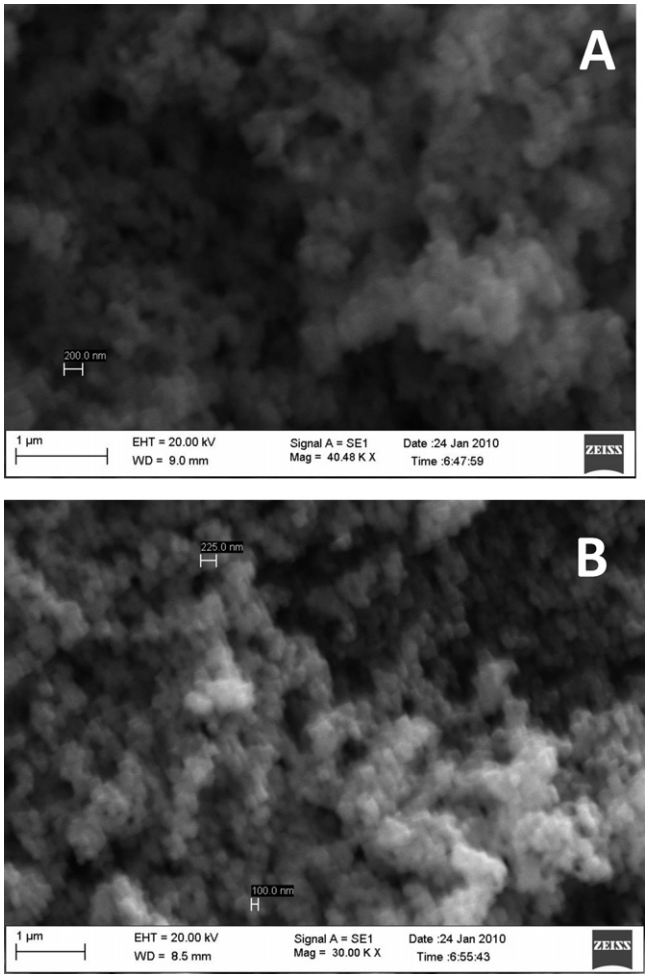

Fig. 3. SEM images of $(TiO_2)_{nps}$ (P-25) (A) and EDAS/$(TiO_2–Au)_{nps}$ (B) nanomaterials annealed at 450 °C.

photogenerated electrons from the $(TiO_2)_{nps}$ to Au_{nps} and thus minimizing the charge recombination of photogenerated electron/hole pair.

3.2. Morphology of EDAS supported $(TiO_2–Au)_{nps}$ nanocomposite material

The TEM images of $(TiO_2)_{nps}$, $(TiO_2–Au)_{nps}$ and EDAS/$(TiO_2–Au)_{nps}$ at same magnifications are given in Fig. 2. The TEM image of TiO_2 nanoparticles shows spherical particles (Fig. 2(A)). The TEM image of the $(TiO_2–Au)_{nps}$ shows the distribution of larger size Au_{nps} on TiO_2 surface (Fig. 2(B)). The TEM image of the EDAS/$(TiO_2–Au)_{nps}$ (Fig. 2(C)) shows the formation of smaller size Au_{nps}, which are highly dispersed on the surface of the TiO_2. The presence of EDAS silicate on TiO_2 facilitates the formation and dispersion of smaller Au_{nps} on the TiO_2. The ultimate contact between Au_{nps} and $(TiO_2)_{nps}$ is more advantageous to increase the interfacial electron transfer process. Both Au_{nps} and $(TiO_2)_{nps}$ undergo fermi level equilibration and as a result the interfacial charge transfer process increases significantly [49].

The SEM images of the $(TiO_2)_{nps}$ and EDAS/$(TiO_2–Au)_{nps}$ with same magnification are shown in Fig. 3. The nanocomposite materials show highly porous like structure and this porous structure may facilitates the diffusion of substrate into the pinholes and create the ultimate contact with the photocatalyst. The EDAX analysis of bare TiO_2 and EDAS/$(TiO_2–Au)_{nps}$ nanocomposite materials were recorded and are shown in Fig. S4. The emission peaks corresponding to the elements O and Ti were observed at 0.5 (O) and 4.5 (Ti), respectively for TiO_2. The emission peaks corresponding to the elements O, Si, Au and Ti were observed at 0.5 (O), 1.8 (Si), 2.2 (Au) and 4.5 (Ti), respectively for the EDAS/$(TiO_2–Au)_{nps}$. The EDAX clearly conforms the presence of elements such as Si, Ti, O and Au in EDAS/$(TiO_2–Au)_{nps}$. The Au content in the EDAS/$(TiO_2–Au)_{nps}$ was calculated as 1.08 wt.%.

Table 1
BET surface analysis of photocatalysts.

Photocatalyst	BET surface area ($m^2\ g^{-1}$)	Average pore diameter (Å)	Pore volume ($cm^3\ g^{-1}$)
TiO_2 (P-25)	43.7	54.30	0.065
$(TiO_2–Au)_{nps}$	48.01	58.03	0.080
EDAS/$(TiO_2–Au)_{nps}$	48.12	67.29	0.083

3.3. BET surface area analysis

The surface area, pore size and pore volume were measured for $(TiO_2)_{nps}$, $(TiO_2–Au)_{nps}$ and EDAS/$(TiO_2–Au)_{nps}$ using BET surface area analysis. The BET surface area analysis data are summarized in Table 1 and their corresponding plots are presented in Fig. S5. Table 1 shows that $(TiO_2–Au)_{nps}$ nanomaterial shows higher surface area and pore volume than that of the bare TiO_2. The porosity of the $(TiO_2–Au)_{nps}$ in the presence and absence of EDAS silicate sol-gel matrix are almost the same. The SEM images of the nanomaterials (Fig. 3) shows that the materials are obviously macroporous and that the N_2-soprtion data prove the presence of micro and mesoporosity (Fig. S5).

3.4. XRD pattern of EDAS/$(TiO_2–Au)_{nps}$

The XRD patterns of $(TiO_2)_{nps}$, $(TiO_2–Au)_{nps}$ and EDAS/$(TiO_2–Au)_{nps}$ nanomaterial films annealed at 450 °C were recorded and are shown in Fig. S6. The XRD pattern showed highly crystallized anatase TiO_2 corresponding to (1 0 1), (0 0 4), (2 0 0), (1 0 5), and (2 1 1) diffractions at 25.3°, 37.8°, 48.1°, 53.9°, and 55.1° (2θ value), respectively (JCPDS No. 86-1156) and (310) diffraction at 64.4° for rutile (Fig. S6). All the diffraction peaks of anatase TiO_2 become sharper and stronger indicating that the deposition of Au_{nps} does not alter the TiO_2 crystalline nature. It is evident from the literature [50,51] that an increase in the crystallinity of TiO_2 can usually lead to an improvement in the photodegradation of organic pollutants [50,51]. It should be noted that the peaks around 39.2° and 44.4° (2θ) are clearly observed due to the Au (1 1 1) and (2 0 0) diffractions (JCPDS No. 4-0784). The peak at 64.4° (2θ) indicative of Au (2 2 0) was overlapped by the peak corresponding to rutile (3 1 0) [52,53]. The XRD pattern of EDAS/$(TiO_2–Au)_{nps}$ nanomaterial films annealed at 250 °C and 450 °C were recorded and are shown in Fig. S7. The XRD patterns (Fig. S7) did not show any observable change due to different annealed temperatures as reported in literature [52,53]. The previous reports show that the XRD patterns of TiO_2(P-25) and TiO_2–Au recorded at 300 °C to 500 °C reveal the diffractions due to anatase and rutile TiO_2 and the TiO_2 was found to stable when Au was deposited on TiO_2 and the annealing at 500 °C did not change the content and particle size of TiO_2 in $(TiO_2–Au)$ samples [52,53]. The $(TiO_2)_{nps}$ crystallite size (25 nm) calculated from the full width at half-maximum (fwhm) of $(TiO_2)_{nps}$ (1 0 1) diffraction peak at the value of 25.3° (2θ) by using the Scherrer equation.

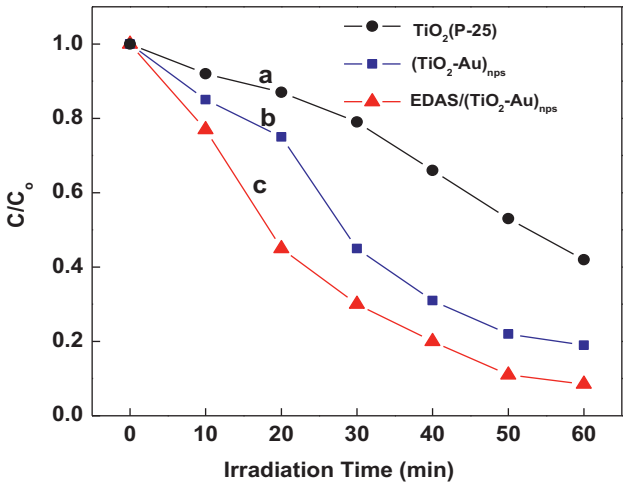

Fig. 4. Photocatalytic reduction of Cr(VI) in the presence of oxalic acid at $(TiO_2)_{nps}$ (P-25) (a), $(TiO_2–Au)_{nps}$ (b) and EDAS/$(TiO_2–Au)_{nps}$ (c) films under irradiation. Concentration of Cr(VI) = 0.4 mM and oxalic acid = 4 mM.

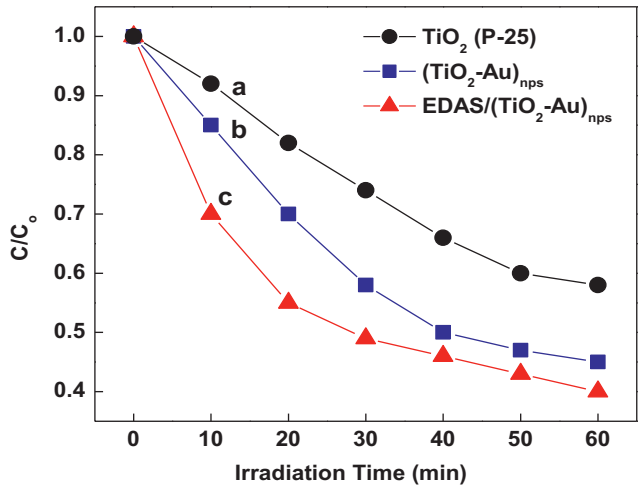

Fig. 6. Photocatalytic oxidation of MB in the absence of Cr(VI) at $(TiO_2)_{nps}$ (P-25) (a), $(TiO_2–Au)_{nps}$ (b) and EDAS/$(TiO_2–Au)_{nps}$ (c) films under irradiation. Concentration of methylene blue = 4 mM.

3.5. *Photocatalytic activity of $(TiO_2–Au)_{nps}$ nanomaterials*

The photocatalytic activity of the EDAS/$(TiO_2–Au)_{nps}$ nanocomposite film was studied using Cr(VI) ions in the presence of oxalic acid or MB dye as a sacrificial electron donor under irradiation. The concentration of the sacrificial electron donor (SD) (oxalic acid) used in this study is based on the molar ratio of Cr(VI):SD = 1:5, which is slightly higher than that of the theoretical requirement ratio of 1:3. In the present study, oxalic acid was used as a sacrificial electron donor to reduce the Cr(VI) to Cr(III) in aqueous solution (Eq. (1)).

$$Cr_2O_7^{2-} + 14\,H^+ + 6\,e^- \rightarrow 2\,Cr^{3+} + 7\,H_2O \quad (1)$$

The change in the concentration of Cr(VI) with respect to irradiation time is shown in Fig. 4. The EDAS/$(TiO_2–Au)_{nps}$ nanocomposite photocatalyst film exhibited significantly faster photocatalytic reduction of Cr(VI) to Cr(III) when compared to the catalytic activity of $(TiO_2)_{nps}$ (P-25) and $(TiO_2–Au)_{nps}$ (Fig. 5). Among the three photocatalyst, the EDAS/$(TiO_2–Au)_{nps}$ showed 91.5% of Cr(VI) reduction to Cr(III) when oxalic acid was used as SD with 1 h irradiation (Fig. 4). The photocatalytic reduction of Cr(VI) was also carried out in the presence of MB dye as SD. The time dependent concentration change observed for Cr(VI) at different nanocomposite photocatalyst films are shown in Fig. 5. A marked synergistic effect was observed at the EDAS/$(TiO_2–Au)_{nps}$ for the photocatalytic reduction of Cr(VI) and oxidation of methylene blue. The extend of synergy depends on the effective interfacial charge transfer between TiO_2 and Cr(VI) through Au_{nps}. The smaller size Au_{nps} deposited on TiO_2 in the presence of EDAS silicate sol–gel improves the photocatalytic reduction and oxidation reactions. The bare $(TiO_2–Au)_{nps}$ film exhibited 54% decrease of Cr(VI) to Cr(III) after 1 h irradiation and the EDAS/$(TiO_2–Au)_{nps}$ showed the same decrease within 20 min. The increase in the photocatalytic reduction of Cr(VI) to Cr(III) and photodegradation of MB dye are attributed to the presence of Au_{nps} on the surface of $(TiO_2)_{nps}$ photocatalyst and its dispersion in the functionalized EDAS silicate sol–gel film. The effective photoinduced charge transfer process between TiO_2 and Au_{nps} minimizes the recombination of the photogenerated charge carriers [8,19]. The increase in the photocatalytic conversion of carcinogenic Cr(VI) to nontoxic Cr(III) coupled with the photodegradation of pollutant MB dye shows the dual benefits of the newly synthesized EDAS/$(TiO_2–Au)_{nps}$ in the film state and its application in the environmental remediation and purification processes.

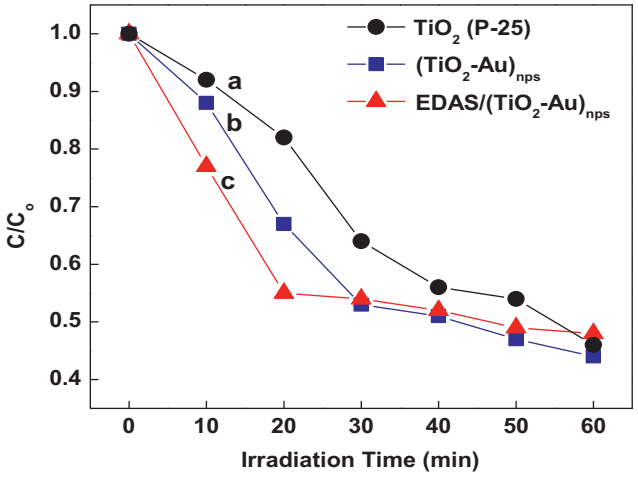

Fig. 5. Photocatalytic reduction of Cr(VI) in the presence of methylene blue at $(TiO_2)_{nps}$ (P-25) (a), $(TiO_2–Au)_{nps}$ (b) and EDAS/$(TiO_2–Au)_{nps}$ (c) films under irradiation. Concentration of Cr(VI) = 0.4 mM and methylene blue = 4 mM.

Figs. 6 and 7 show the photocatalytic degradation of MB at different time under irradiation using $(TiO_2)_{nps}$, $(TiO_2–Au)_{nps}$ and EDAS/$(TiO_2–Au)_{nps}$ films both in the absence and presence of Cr(VI). The decrease in the MB dye concentration with respect to time clearly shows the degradation of MB molecules due to the fragmentation of MB leading to the decoloration of dye under illumination. It is known that the conjugated structure of MB is broken into small aromatic intermediates [54,55]. The 49% photodegradation of MB dye in the presence of Cr(VI) at the EDAS/$(TiO_2–Au)_{nps}$ film required only 10 min when compared to $(TiO_2)_{nps}$ and $(TiO_2–Au)_{nps}$ films in the absence of EDAS (Fig. 7). Under similar experimental condition, 60% photodegradation of MB dye required 1 h in the absence of Cr(VI) at the bare $(TiO_2)_{nps}$ and $(TiO_2–Au)_{nps}$ films (Fig. 6). Varying the concentration of Cr(VI) did not affect the MB degradation and varying the concentration of MB affected the Cr(VI) reduction.

The decrease in total organic carbon (TOC) content observed during the photocatalytic degradation of MB in the absence of Cr(VI) (Fig. 8) and in the presence of Cr(VI) (Fig. 9) using $(TiO_2)_{nps}$, $(TiO_2–Au)_{nps}$ and EDAS/$(TiO_2–Au)_{nps}$ films under irradiation is plotted against the time. In the absence of Cr(VI), the mineralization of MB dye reached the highest value in 20 min of irradiation at the EDAS/$(TiO_2–Au)_{nps}$ film. However, in the presence of Cr(VI) the mineralization of MB dye reached the highest value in about 10 min

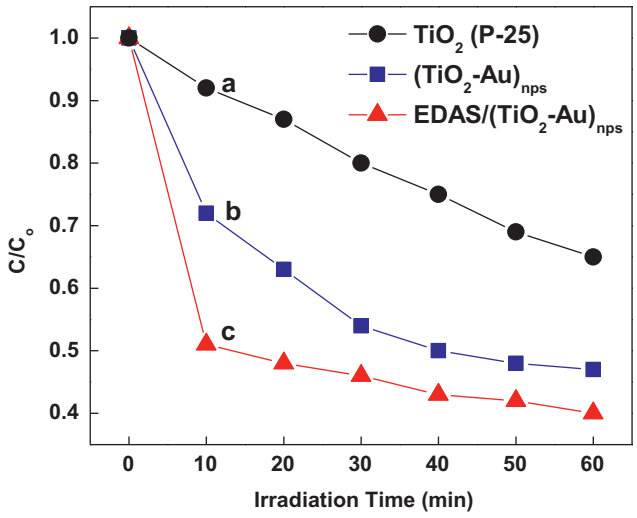

Fig. 7. Photocatalytic oxidation of MB in the presence of Cr(VI) at $(TiO_2)_{nps}$ (P-25) (a), $(TiO_2–Au)_{nps}$ (b) and EDAS/$(TiO_2–Au)_{nps}$ (c) films under irradiation. Concentration of Cr(VI) = 0.4 mM and methylene blue = 4 mM.

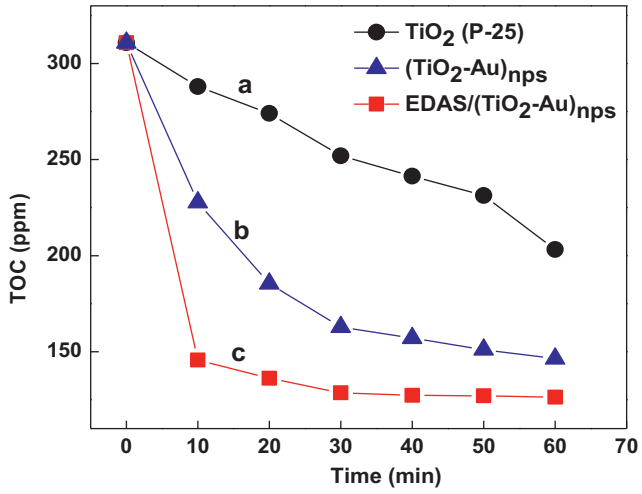

Fig. 9. Photocatalytic mineralization of methylene blue in the presence of Cr(VI) ions at $(TiO_2)_{nps}$ (P-25) (a), $(TiO_2–Au)_{nps}$ (b) and EDAS/$(TiO_2–Au)_{nps}$ (c) films under irradiation. Concentration of Cr(VI) = 0.4 mM and methylene blue = 4 mM.

at the EDAS/$(TiO_2–Au)_{nps}$. The photocatalytic mineralization of MB dye was found to be higher at the EDAS/$(TiO_2–Au)_{nps}$ film when compared to $(TiO_2)_{nps}$ (P-25) and $(TiO_2–Au)_{nps}$ film (Figs. 8 and 9). This is mainly attributed to the effective simultaneous utilization of photoinduced holes/electrons at the EDAS/$(TiO_2–Au)_{nps}$ film. The increased photocatalytic performance is mainly attributed to the presence of Au_{nps} on the $(TiO_2)_{nps}$ surface since the Au_{nps} act as an electron sink for the photogenerated electrons and minimizes the charge recombination process [19]. The Au_{nps} is a well known electron conductor and catalyst, and hence the photogenerated electrons are rapidly transferred from $(TiO_2)_{nps}$ to the Cr(VI) through the Au_{nps} [8,19]. The holes formed at the $(TiO_2)_{nps}$ oxidize the sacrificial electron donor MB. The deposition of Au_{nps} on $(TiO_2)_{nps}$ also decreases the band-gap energy of $(TiO_2)_{nps}$ leading to the absorption of visible light by the $(TiO_2)_{nps}$.

The schematic representation of the photocatalyzed simultaneous reduction–oxidation reaction occurring at the EDAS/$(TiO_2–Au)_{nps}$ film as shown in Fig. S8. When the EDAS/$(TiO_2–Au)_{nps}$ is irradiated with light, the charge separation (h^+/e^-) occurs at the $(TiO_2)_{nps}$. The conduction band electrons are rapidly transferred to the Au_{nps} at the interface. The Au_{nps} instantaneously transfer the electrons to reduce the Cr(VI) to Cr(III) and the holes at the valance band of the $(TiO_2)_{nps}$ oxidize the sacrificial electron donor MB dye. The Au_{nps} act as an electron sink and plays a vital role in the photocatalytic activity by facilitating effective interfacial charge transfer process leading to the simultaneous photocatalytic reduction and oxidation processes. This simultaneous photocatalytic reduction and oxidation processes provides the dual benefits for the environmental remediation and purification processes.

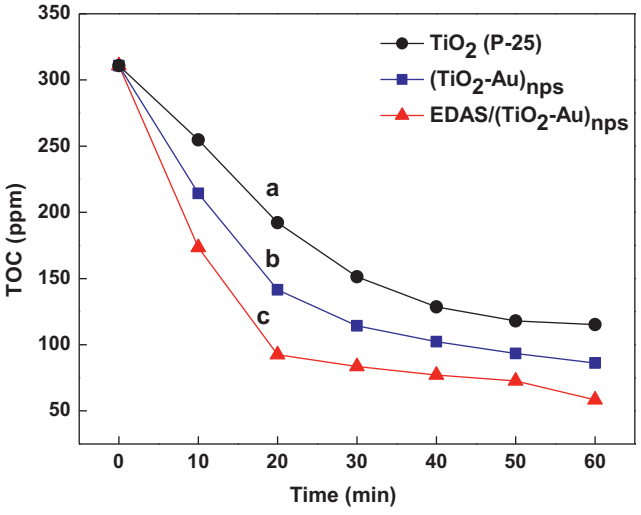

Fig. 8. Photocatalytic mineralization of methylene blue in the absence of Cr(VI) ions at $(TiO_2)_{nps}$ (P-25) (a), $(TiO_2–Au)_{nps}$ (b) and EDAS/$(TiO_2–Au)_{nps}$ (c) films under irradiation. Concentration of methylene blue = 4 mM.

4. Summary

In summary, the diamine functionalized EDAS silicate sol–gel supported nanocomposite $(TiO_2–Au)_{nps}$ material was prepared by a simple deposition–precipitation method and characterized by DRS, TEM, SEM, EDAX, BET and XRD analysis. The smaller Au_{nps} were deposited on the EDAS/TiO_2 than on the bare TiO_2. The dispersion $(TiO_2–Au)_{nps}$ into EDAS silicate sol–gel paves the way to prepare solid-phase EDAS/$(TiO_2–Au)_{nps}$ in the film state. This photocatalyst film was utilized for the simultaneous photoinduced reduction and oxidation of pollutants like Cr(VI) and MB dye, respectively. The presence of smaller Au_{nps} on the $(TiO_2)_{nps}$ surface effectively improves the synergistic action in the photocatalytic reduction of Cr(VI) to Cr(III) and the photocatalytic oxidation of MB dye when compared to the bare $(TiO_2)_{nps}$. The EDAS/$(TiO_2–Au)_{nps}$ nanocomposite solid-phase photocatalyst is a potential candidate for environmental remediation and purification processes through the photoinduced advanced oxidation–reduction processes.

Acknowledgments

RR acknowledges the financial support from the Department of Science and Technology (DST), New Delhi. APK is a recipient of CSIR-Senior Research Fellow fellowship. The authors are grateful to Evonik Industries, Germany for generously providing the TiO_2 (Degussa P-25) sample for research purpose. Dr. S. Murugesan, School of Chemistry, Madurai Kamaraj University for TOC measurements and Mr. S. Suresh for his help. We thank Dr. M.L.P. Reddy, Scientist, NIIST, Thiruvananthapuram for providing the BET surface area analysis.

Appendix A. Supplementary data

Supplementary data associated with this article can be found, in the online version, at doi:10.1016/j.jhazmat.2011.12.019.

References

[1] A. Ito, H. Masumoto, T. Goto, Optical properties of Au nanoparticle dispersed TiO_2 films prepared by laser ablation, Mater. Trans. 44 (2003) 1599.
[2] M.L. Steigerwald, L.E. Brus, Semiconductor crystallites: a class of large molecules, Acc. Chem. 23 (1990) 183.
[3] Y. Wu, K. Sun, J. Yu, B. Xu, A key to the storage stability of Au/TiO_2 catalyst, Phys. Chem. Chem. Phys. 10 (2008) 6399.
[4] Z. Bian, J. Zhu, F. Cao, Y. Lu, H. Li, In-situ encapsulation of Au nanoparticles in mesoporous core–shell TiO_2 microspheres with enhanced activity and durability, Chem. Commun. (2009) 3789.
[5] P.V. Kamat, Meeting the clean energy demand: nanostructure architectures for solar energy conversion, J. Phys. Chem. C 111 (2007) 2834.
[6] P.V. Kamat, D. Meisel, Nanoscience opportunities in environmental remediation, C. R. Chimie 6 (2003) 999.
[7] Y. Zhang, A.H. Yuwono, J. Lib, J. Wang, Highly dispersed gold nanoparticles assembled in mesoporous titania films of cubic configuration, Microporous Mesoporous Mater. 110 (2008) 242.
[8] H. Li, Z. Bian, J. Zhu, Y. Huo, H. Li, Y. Lu, Mesoporous Au/TiO_2 nanocomposites with enhanced photocatalytic activity, J. Am. Chem. Soc. 129 (2007) 4538.
[9] A. Pandikumar, R. Ramaraj, Aminosilicate sol–gel embedded core-shell $(TiO_2–Au)_{nps}$ nanomaterials modified electrode for the electrochemical detection of nitric oxide, Ind. J. Chem. A 50A (2011), 1388.
[10] Y. Wang, D. Zhao, W. Ma, C. Chen, J. Zhao, Enhanced sonocatalytic degradation of azo dyes by Au/TiO_2, Environ. Sci. Technol. 42 (2008) 6173.
[11] P.C. Lansåker, J. Backholm, G.A. Niklasson, C.G. Granqvist, TiO_2/Au/TiO_2 multilayer thin films: novel metal-based transparent conductors for electrochromic devices, Thin Solid Films 518 (2009) 1125.
[12] Y. Tian, T. Tatsuma, Mechanisms and applications of plasmon-induced charge separation at TiO_2 films loaded with gold nanoparticles, J. Am. Chem. Soc. 127 (2005) 7632.
[13] A. Pandikumar, S. Murugesan, R. Ramaraj, Functionalized silicate sol–gel supported TiO_2–Au core–shell nanomaterials and their photoelectrocatalytic activity, ACS Appl. Mater. Interfaces 2 (2010) 1912.
[14] C. Chou, R. Yang, C. Yeh, Y. Lin, Preparation of TiO_2/Nano-metal composite particles and their applications in dye-sensitized solar cells, Powder Technol. 194 (2009) 95.
[15] Y. Qu, H. Min, Y. Wei, F. Xiao, G. Shi, X. Li, L. Jin, Au–TiO_2/Chit modified sensor for electrochemical detection of trace organophosphates insecticides, Talanta 76 (2008) 758.
[16] D. Buso, M. Post, C. Cantalini, P. Mulvaney, A. Martucci, Gold nanoparticle-doped TiO_2 semiconductor thin films: gas sensing properties, Adv. Funct. Mater. 18 (2008) 3843.
[17] M. Nishibori, W. Shin, K. Tajima, L.F. Houlet, N. Izu, T. Itoh, S. Tsubota, I. Matsubra, Thermoelectric gas sensor using Au loaded titania CO oxidation catalyst, J. Ceram. Soc. Jpn. 115 (2007) 37.
[18] M.G. Manera, J. Spadavecchia, D. Buso, C.D. Julián Fernández, G. Mattei, A. Martucci, P. Mulvaney, J. Pérez-Juste, R. Rella, L. Vasanelli, P. Mazzoldi, Optical gas sensing of TiO_2 and TiO_2/Au nanocomposite thin films, Sens. Actuators B: Chem. 132 (2008) 107.
[19] A. Dawson, P.V. Kamat, Semiconductor–metal nanocomposites. Photoinduced fusion and photocatalysis of gold-capped TiO_2 (TiO_2/Gold) nanoparticles, J. Phys. Chem. B 105 (2001) 960.
[20] Y. Nosaka, K. Norimatsu, H. Miyama, The function of metals in metal-compounded semiconductor photocatalysts, Chem. Phys. Lett. 106 (1984) 128.
[21] J. Giménez, M.A. Aguado, S. Cervera-March., Photocatalytic reduction of chromium(VI) with titania powders in a flow system. Kinetics and catalyst activity, J. Mol. Catal. A: Chem. 105 (1996) 67.
[22] Y. Ku, I. Jung, Photocatalytic reduction of Cr(VI) in aqueous solutions by UV irradiation with the presence of titanium dioxide, Water Res. 35 (2001) 135.
[23] R. Vinu, G. Madras, Kinetics of simultaneous photocatalytic degradation of phenolic compounds and reduction of metal ions with nano-TiO_2, Environ. Sci. Technol. 42 (2008) 913.
[24] B. Sun, E.P. Reddy, P.G. Smirniotis, Visible light Cr(VI) reduction and organic chemical oxidation by TiO_2 photocatalysis, Environ. Sci. Technol. 39 (2005) 6251.
[25] J. Testa, M. Grela, M. Litter, Heterogeneous photocatalytic reduction of chromium(VI) over TiO_2 particles in the presence of oxalate: involvement of Cr(V) species, Environ. Sci. Technol. 38 (2004) 1589.
[26] X. Wang, S.O. Pehkonen, A.K. Ray, Removal of aqueous Cr(VI) by a combination of photocatalytic reduction and coprecipitation, Ind. Eng. Chem. Res. 43 (2004) 1665.
[27] C.R. Chenthamarakshan, K. Rajeshwar, E.J. Wolfrum, Heterogeneous photocatalytic reduction of Cr(VI) in UV-irradiated titania suspensions: effect of protons, ammonium ions, and other interfacial aspects, Langmuir 16 (2000) 2715.
[28] N. Wang, Y. Xu, L. Zhu, X. Shen, H. Tang, Reconsideration to the deactivation of TiO_2 catalyst during simultaneous photocatalytic reduction of Cr(VI) and oxidation of salicylic acid, J. Photochem. Photobiol. A: Chem. 201 (2009) 121.
[29] H. Kyung, J. Lee, W. Choi, Simultaneous and synergistic conversion of dyes and heavy metal ions in aqueous TiO_2 suspensions under visible-light illumination, Environ. Sci. Technol. 39 (2005) 2376.
[30] X.R. Xu, H.B. Li, J.D. Gu, Photocatalytic reduction of hexavalent chromium and degradation of di-n-butyl phthalate in aqueous TiO_2 suspensions under ultraviolet light, Environ. Tech. 28 (2007) 1055.
[31] J. Yoon, E. Shim, H. Joo, Photocatalytic reduction of hexavalent chromium (Cr(VI)) using rotating TiO_2 mesh, Korean J. Chem. Eng. 26 (2009) 1296.
[32] P. Mohapatra, S.K. Samantaray, K. Parida, Photocatalytic reduction of hexavalent chromium in aqueous solution over sulphate modified titania, J. Photochem. Photobiol. A: Chem. 170 (2005) 189.
[33] H. Yu, S. Chen, X. Quan, H. Zhao, Y. Zhang, Fabrication of a TiO_2–BDD heterojunction and its application as a photocatalyst for the simultaneous oxidation of an azo dye and reduction of Cr(VI), Environ. Sci. Technol. 42 (2008) 3791.
[34] P. Kajitvichyanukul, J. Ananpattarachai, S. Pongpom, Sol–gel preparation and properties study of TiO_2 thin film for photocatalytic reduction of chromium(VI) in photocatalysis process, Tech. Adv. Mater. 6 (2005) 352.
[35] G.C.C. Yang, S.W. Chan, Photocatalytic reduction of chromium(VI) in aqueous solution using dye sensitized nanoscale ZnO under visible light irradiation, J. Nanopart. Res. 11 (2009) 230.
[36] S. Chakrabarti, B. Chaudhuri, S. Bhattacharjee, A.K. Ray, B.K. Dutta, Photoreduction of hexavalent chromium in aqueous solution in the presence of zinc oxide as semiconductor catalyst, Chem. Eng. J. 153 (2009) 86.
[37] E. Gkika, A. Troupis, A. Hiskia, Papaconstantinou, Photocatalytic reduction of chromium and oxidation of organics by polyoxometalates, Appl. Catal. B 62 (2006) 28.
[38] S. Kim, J. Yeo, W. Choi, Simultaneous conversion of dye and hexavalent chromium in visible light-illuminated aqueous solution of polyoxometalate as an electron transfer catalyst, Appl. Catal. B 84 (2008) 148.
[39] S. Rengaraj, S. Venkataraj, J. Yeon, Y. Kim, X.Z. Li, G.K.H. Pang, Preparation, characterization and application of Nd–TiO_2 photocatalyst for the reduction of Cr(VI) under UV light illumination, Appl. Catal. B 77 (2007) 157.
[40] S.X. Liu, Z.P. Qu, X.W. Han, C.L. Sun, A mechanism for enhanced photocatalytic activity of silver-loaded titanium dioxide, Catal. Today 93–95 (2004) 877.
[41] J.A. NavõÂoa, G. ColoÂna, M. Trillasb, J. Peralb, X. DomeÁnechb, J.J. Testac, J. PadroÂnc, D. RodrõÂguezc, M.I. Litterc, Heterogeneous photocatalytic reactions of nitrite oxidation and Cr(VI) reduction on iron-doped titania prepared by the wet impregnation method, Appl. Catal. B 16 (1998) 187–196.
[42] L. Yang, Y. Xiao, S. Liu, Y. Li, Q. Cai, S. Luo, G. Zeng, Photocatalytic reduction of Cr(VI) on WO_3 doped long TiO_2 nanotube arrays in the presence of citric acid, Appl. Catal. B 94 (2010) 142.
[43] N. Wang, L. Zhu, K. Deng, Y. She, Y. Yu, H. Tang, Visible light photocatalytic reduction of Cr(VI) on TiO_2 in situ modified with small molecular weight organic acids, Appl. Catal. B 95 (2010) 400.
[44] G. Liao, S. Chen, X. Quan, H. Chen, Y. Zhang, Photonic crystal coupled TiO_2/polymer hybrid for efficient photocatalysis under visible light irradiation, Environ. Sci. Technol. 44 (2010) 3481.
[45] K. Ueno, T. Imamura, K.L. Cheng, Handbook of Organic Analytical Reagents, CRC Press, Boca Raton, FL, 1992, p. 339.
[46] N.M. Stover, Diphenyl carbazide as a test for chromium, J. Am. Chem. Soc. 50 (1928) 2363.
[47] M. Gartner, V. Dremov, P. Muller, H. Kisch, Bandgap widening of titania through support interactions, Chem. Phys. Chem. 6 (2005) 714.
[48] Y. Liu, L. Chen, J. Hu, J. Li, R. Richards, TiO_2 nanoflakes modified with gold nanoparticles as photocatalysts with high activity and durability under near UV irradiation, J. Phys. Chem. C 114 (2010) 1641.
[49] M. Jakob, H. Levanon, P.V. Kamat, Charge distribution between UV-irradiated TiO_2 and gold nanoparticles: determination of shift in the fermi level, Nano Lett. 3 (2003) 353.
[50] B. Ohtani, S. Nishimoto, Effect of surface adsorptions of aliphatic alcohols and silver ion on the photocatalytic activity of titania suspended in aqueous solutions, J. Phys. Chem. 97 (1993) 920.
[51] G. Tian, H. Fu, L. Jing, B. Xin, K. Pan, Preparation and characterization of stable biphase TiO_2 photocatalyst with high crystallinity, large surface area, and enhanced photoactivity, J. Phys. Chem. C 112 (2008) 3083.
[52] J. Huang, W.-L Dai, H. Li, K. Fan, Au/TiO_2 as high efficient catalyst for the selective oxidative cyclization of 1,4-butanediol to γ-butyrolactone, J. Catal. 252 (2007) 69.
[53] B. Tian, J. Zhang, T. Tong, F. Chen, Preparation of Au/TiO2 catalysts from Au(I)–thiosulfate complex and study of their photocatalytic activity for the degradation of methyl orange, Appl. Catal. B 79 (2008) 394.
[54] T. Zhang, T. Oyama, A. Aoshima, H. Hidaka, J. Zhao, N. Serpone, Photooxidative N-demethylation of metheylene blue in aqueous TiO_2 dispersions under UV irradiation, J. Photobiol. A: Chem. 140 (2001) 163.
[55] A. Houas, H. Lachheb, M. Ksibi, E. Elaloui, C. Guillard, J.M. Herrmann, Photocatalytic degradation pathway of methylene blue in water, Appl. Catal. B 31 (2001) 145.